University of Nebraska - Lincoln

# DigitalCommons@University of Nebraska - Lincoln

# Atomic photoionization by multiple temporal pairs of slits

Jean Marcel Ngoko Djiokap

# Atomic photoionization by multiple temporal pairs of slits

J. M. Ngoko Djiokap

*Department of Physics and Astronomy, University of Nebraska, Lincoln, Nebraska 68588-0299, USA*

We study interactions between multiple temporal pairs of slits in coherent control of photoionization of *S*-state atoms using a pulse train of $N + 1$ pairs evenly delayed in time by $\tau$, in which the two pulses in a pair with a delay $\tau_0$ are counter-rotating circularly polarized. For interacting two double-slit experiments, while Ramsey interference between two identical Archimedean spirals yields pairs of principal spirals, interference of two spirals with opposite handedness does not lead to spirals, but instead to crocodile-eye-like patterns with nictares. For more than two interacting experiments, the resulting patterns turn out just to be those two reference patterns modulated by different kinds of $N$-dependent time-energy Fraunhofer functions exhibiting diffraction-grating-like patterns.

## I. INTRODUCTION

Wave-particle duality is one of the pivotal concepts of quantum mechanics, which has been historically demonstrated by a series of landmark experiments and proposals. Whereas the 1801 Young's space double-slit interference experiment [1] demonstrated the wave nature of light, Einstein's explanation of the photoelectric effect [2] in 1905 followed by Compton's light scattering experiment [3] in 1923 introduced firm evidence of the particle nature of light. The de Broglie's hypothesis [4] in 1924 and the subsequent electron-diffraction experiments [5] in 1927 by Davisson and Germer established the wave nature of the electron. Diffraction grating (viewed as a large number of evenly spaced parallel slits) was first developed by Fraunhofer in 1821. A version of the two-slit experiment with a single electron [6] was first performed in 1961 by Jönsson, who studied 13 years later electron diffraction at multiple slits [7]. In recent years, time double-slit experiments (the counterpart of space double-slit experiments) with electrons from ionization using time-delayed femtosecond laser pulses [8] or a few-cycle infrared field with stable and tunable carrier-envelope-phase (CEP) [9] have been realized, providing further confirmation of wave-particle duality.

In the time two-slit scheme [8] but with circularly polarized (CP) extreme ultraviolet (XUV) attosecond pulses, an unusual kind of Ramsey interference [10] of electron wave packets following photoionization of He was predicted in 2015 to lead to a novel electron phenomenon [11]. It was found that the momentum distribution in the polarization plane exhibits either two-arm Archimedean spiral vortex structures (for counter-rotating pulses) or Newton's rings (for corotating pulses). A year later, control of the number of spiral arms was achieved in multiphoton single ionization of He by both single-color and two-color time-delayed CP pulses [12]. It was demonstrated that the number of spiral arms depends upon the number of photons required for single ionization of atoms. As those spiral patterns from single ionization of atoms by single-

color fields have a counterpart in optics [13] when interfering particular kinds of laser beams, the predictions [11,12] provided another example of wave-particle duality. The predictions [11,12] have now been confirmed experimentally in multiphoton ionization of potassium atoms using single-color time-delayed CP femtosecond pulses [14,15] and of sodium atoms using bichromatic counter-rotating or corotating CP cycloidal femtosecond laser fields [16,17].

All these work have stimulated numerous theoretical studies for the occurrence of the same pattern in other systems and processes (see, e.g., Refs. [18–30]). While spiral patterns occur in ionization processes in the perturbative multiphoton regime [18–21,26,27,29,30], they also occur in the strong-field tunneling regime [23–25,28]. In particular, Ref. [22] reported on momentum vortices even in pairs production by two counter-rotating fields. Photoionization of single-electron molecular systems such as $H_2^+$ [18] and $H_3^{2+}$ [19] by bichromatic CP fields was found to lead to spiral patterns even for corotating fields. These results predicted in molecules have been confirmed in atoms [12]. Whether this electron phenomenon occurs only in uncorrelated processes has been addressed by considering correlated processes such as double ionization of a He atom [20,21] or $H_2$ molecule [26,30] by one-photon transition [20,26] or by two-photon transition [21,30]. It was shown that spiral patterns emerge in two-electron momentum distributions for only a particular class of detection geometries in which the mutual angle of the two photoelectrons is fixed during the particle detection.

All these studies on spiral electron vortices made use of a pair of time-delayed copropagating counter-rotating or corotating *isolated* pulses, but never a train of pulses. Of note is that Ref. [29] used two crossing polarized ultrashort pulses. The possibility of investigating atomic ionization using pulse trains opens a doorway into manipulating interactions between several temporal two-slit experiments that could lead to novel physics and applications. Potential applications of
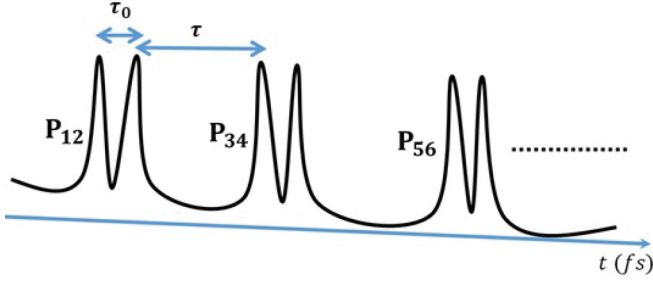
FIG. 1. Sketch of a train of $N+1$ pairs of CP pulses, delayed in time by $\tau$. In each pair, $P_{j\,j+1}$, where $j = 1, 3, 5, \ldots$, the two pulses delayed in time by $\tau_0$ are counter-rotating. Here $\tau > \tau_0$ for illustration, but $\tau$ and $\tau_0$ can be chosen arbitrarily. The *temporal* structure of this train is similar to high-harmonic generation *energy* spectra exhibiting pairs of $3n + 1$ and $3n + 2$ CP harmonics with alternating helicities created by bicircular field drivers [32]. For $\tau_0 = 0$, each pair of pulses becomes a linearly polarized pulse, and this train reduces to one similar to the first ever created train of attosecond pulses [33].

such studies include pulse diagnosis with an emphasis on polarization photodetector, a reference pattern for attosecond chronoscopy of photoemission, attosecond quantum beats and optical switches, and electron grating spectrometers.

In this paper, we use a pulse train of $N+1$ pairs $P_{j\,j+1}$ (see Fig. 1) evenly delayed in time by $\tau$ (in which the two pulses in a pair are delayed in time by $\tau_0$) to study interactions between multiple temporal two-slit interference patterns produced in coherent control of the linear process of photoionization of $S$-state atoms. Below we focus on two kinds of trains of CP pulse pairs that differ only by their helicities, with each pulse in a pair having the same carrier frequency $\omega$ larger than $E_b$ (the binding energy) and an intensity $I_0$ such that the valid first-order perturbation theory (PT) can fully analyze results from the time-dependent Schrödinger equation (TDSE) calculations. In contrast to previous work [18,19] where recollisions with parent ions may be present when bichromatic counter-rotating pulses are used [31], the use of single-color few-cycle XUV CP fields here precludes any recollision process. For train I where each pair has right-left circularly polarized (RLCP) pulses or left-right circularly polarized (LRCP) pulses, the interaction of identical spiral patterns yields pairs of principal and secondary spirals, stemming from diffraction-grating-like patterns modulating the reference pattern of two-arm Archimedean spiral. The intensity, width, and number of these resulting spiral pairs can be exquisitely controlled by varying $N$, $\tau$, and the pulse duration $T$. All these results are for coherent pulses with zero CEPs; a two-arm roller coaster spiral is shown to be formed when varying the CEPs for the case $N = 1$. For train II where successive pairs are made of RLCP and LRCP pulses, interaction of these two spiral patterns with opposite handedness does not give rise to spirals, but instead to crocodile-eye-like patterns with nictares.

This paper is organized as follows. In Sec. II our numerical procedure for obtaining the triply differential probability is briefly described. In Sec. III we present our analytical and numerical results for the interaction between two kinds of spiral patterns. While Sec. III A is devoted to interaction of

several spiral patterns with the same handedness, Sec. III A discusses interaction of several spiral patterns with opposite handedness. In Sec. IV a brief summary of the derived results is provided. In Appendix A a sensitivity of the generated spiral pairs to the time delay $\tau$ and pulse duration $T$ is presented. Meanwhile, the dependence of the generated spiral pairs to the pulse CEP is discussed in Appendix B. Atomic units (a.u.) are used throughout the text unless otherwise specified.

## II. NUMERICAL METHOD

In this section, our numerical procedure for obtaining the triply differential probability for photoionization of $S$-state atoms by the pulse train in Fig. 1 is briefly described. The electric field of such pulse trains of $N+1$ pairs is

$$\mathbf{F}(t) = \frac{1}{2} \sum_n [F_0(t - n\tilde{\tau})e^{-i\omega(t-n\tilde{\tau})}\mathbf{e}_{\phi_{2n+1}} $$
$$+ F_0(\tilde{t} - n\tilde{\tau})e^{-i\omega(\tilde{t}-n\tilde{\tau})}\mathbf{e}_{\phi_{2n+2}}] + \text{c.c.}, \quad (1)$$

where $n$ runs from 0 to $N$, $\tilde{t} = t - \tau_0$; $\tilde{\tau} = \tau + \tau_0$; $F_0(t) = \sqrt{I_0}f(t)$, with $f(t)$ being the pulse envelope; and $\mathbf{e}_{\phi_j} = \mathbf{e}_j e^{-i\phi_j}$, where $\mathbf{e}_j = (\hat{\epsilon} + i\eta_j\hat{\zeta})/(1 + \eta_j^2)^{1/2}$ and $\phi_j$ denote, respectively, the polarization vector and CEP of the $j$th pulse in the train. Here $\hat{\epsilon} \equiv \hat{x}$ and $\hat{\zeta} \equiv \hat{y}$ define the major and minor axes of the polarization ellipse, and $|\eta_j|$ is the pulse ellipticity, where $-1 \leqslant \eta_j \leqslant 1$ [34]. Note that while $\eta_j = 0$ for linear polarization, $|\eta_j| < 1$ for elliptical polarization, and $|\eta_j| = 1$ for circular polarization [34]. The sign of $\eta_j$ defines the helicity of the $j$th pulse. Thus, $\eta_j = +1(-1)$ defines a right(left) CP pulse. For the pulse train (1), we solve the TDSE as in [11,12,35,36] to obtain the triply differential probability (TDP),

$$\mathcal{W}_N(\mathbf{p}) = |\langle \Theta_{1s,\mathbf{p}}^{(-)}(\mathbf{r}_1, \mathbf{r}_2)|\Psi(\mathbf{r}_1, \mathbf{r}_2, T_f)\rangle|^2, \quad (2)$$

by projecting the wave packet $\Psi(\mathbf{r}_1, \mathbf{r}_2, t)$ (solution of the TDSE at the end of the train $t = T_f$) onto a field-free state, as the Jacobi matrix scattering wave function $\Theta_{1s,\mathbf{p}}^{(-)}(\mathbf{r}_1, \mathbf{r}_2)$ for He [36].

## III. ANALYTICAL AND NUMERICAL RESULTS

To investigate analytically the interaction between several spiral patterns, we invoke first-order perturbation theory (PT), which applies here since the pulse parameters are such that the ponderomotive energy $U_p \ll \omega$, and the Keldysh parameter $\gamma = \sqrt{E_b/2U_p} \gg 1$. Therefore, the transition amplitude for one-photon ionization within the PT framework writes [37]

$$\mathcal{A} = -i \int dt \, e^{+iE_f t}\langle \nu\mathbf{p}|\mathbf{d} \cdot \mathbf{F}(t)|i\rangle e^{-iE_i t}, \quad (3)$$

where $\mathbf{d}$ is the electric dipole moment operator of the atom, $E_i < 0$ is the energy of the ground state $|i\rangle$, and $E_f = E + E_\nu$ is the energy of the final state $|\nu\mathbf{p}\rangle$, with $E_\nu < 0$ being the energy of the residual ion in an excited state characterized by the principal quantum number $\nu$. Note that $E_f - E_i = E + E_b$, where $E_b = E_\nu - E_i$ is the corresponding atomic binding energy. For such pulse parameters, the rotating wave approximation (RWA) is valid. Thus, it is legitimate to neglect photon

emission processes in PT analysis (3) which are described by the c.c. part of the electric field $\mathbf{F}(t)$ (1). Using the formalism of tensors, a parametrization for the PT amplitude (3) in terms of the polarization vector $\mathbf{e}_j$ and the electron momentum $\mathbf{p} \equiv (p, \hat{\mathbf{p}})$ can be written as [34]

$$
\mathcal{A} = \sum_n e^{i\tilde{\Phi}_n}[\alpha^{(2n+1)}(p)(\mathbf{e}_{2n+1} \cdot \hat{\mathbf{p}})e^{-i\phi_{2n+1}}
$$
$$
+ \alpha^{(2n+2)}(p)(\mathbf{e}_{2n+2} \cdot \hat{\mathbf{p}})e^{-i\phi_{2n+2}}e^{i\Phi_0}], \quad (4)
$$

where $\tilde{\Phi}_n = (E + E_b)n\tilde{\tau}$ is the Ramsey phase accumulated between the births of the electron wave packets created by the zeroth and $n$th pairs of pulses; and $\Phi_0 = (E + E_b)\tau_0$ is the Ramsey phase accumulated between the two electron wave packets created by odd and even pulses in a pair. In Eq. (4) the angular-independent dynamical parameter $\alpha^{(j)}(p)$ is the product of $\sqrt{I_0}$, the electric field strength, $\hat{F}^+(E + E_b - \omega)$, the Fourier transform of the pulse envelope $f(t)$, and $\mu(E)$, the radial part of the transition matrix element between the initial and final states. For a peak intensity $I_0$ considered here, the ground state depletion is negligible so that each pulse in the train sees essentially the same initial ground state. Under such assumption, $\alpha^{(j)}(p) \simeq \alpha(p)$ can be pulled out from the sum in (4). Using the compact notation $\mathbf{e}_{\phi_j} = \mathbf{e}_j e^{-i\phi_j}$, the PT amplitude (4) becomes

$$
\mathcal{A} \simeq \alpha(p) \sum_n e^{i\tilde{\Phi}_n}[(\mathbf{e}_{\phi_{2n+1}} \cdot \hat{\mathbf{p}}) + (\mathbf{e}_{\phi_{2n+2}} \cdot \hat{\mathbf{p}})e^{i\Phi_0}], \quad (5)
$$

where $\alpha(p) \equiv \sqrt{I_0}\mu(E)\hat{F}^+(\epsilon)$, $E = p^2/2$, and $\epsilon \equiv E + E_b - \omega$. The result (5) is general and applied for any polarization state of light and any $S$-state atom. For illustration, below we choose He with $\omega = 36$ eV and $E_b \simeq 24.59$ eV.

### A. Interaction of several two-arm spiral patterns with the same handedness

For train I where each pair is made of either RLCP pulses or LRCP pulses, $\mathbf{e}_{2n+1} \equiv \mathbf{e}_{2n+2}^* \equiv \mathbf{e}$, and Eq. (4) can be rewritten as

$$
\mathcal{A} \simeq \alpha(p) \sum_n q^n e^{-i\phi_{2n+1}}[(\mathbf{e} \cdot \hat{\mathbf{p}}) + (\mathbf{e}^* \cdot \hat{\mathbf{p}})e^{i\psi_n}]. \quad (6)
$$

Here $q = e^{i(E+E_b)\tilde{\tau}}$ and $\psi_n \equiv \Phi_0 + \Delta\phi_n$, where $\Delta\phi_n = \phi_{2n+1} - \phi_{2n+2}$. The geometric factor $(\mathbf{e} \cdot \hat{\mathbf{p}})$ in terms of the spherical angles $(\theta, \varphi)$ for the momentum $\mathbf{p}$ is

$$
(\mathbf{e} \cdot \hat{\mathbf{p}}) = \frac{\sin\theta}{\sqrt{2}} e^{-i\xi\varphi}, \quad (7)
$$

where $\xi = +1(-1)$ for RLCP (LRCP) pulses. Substituting Eq. (7) into Eq. (6), one obtains

$$
\mathcal{A} \simeq [\alpha(p)/\sqrt{2}] \sin\theta \sum_n q^n e^{i(\psi_n/2 - \phi_{2n+1})}
$$
$$
\times \{e^{i(\psi_n/2 - \xi\varphi)} + e^{-i(\psi_n/2 - \xi\varphi)}\}. \quad (8)
$$

The term in this curly bracket is $2\cos(\psi_n/2 - \xi\varphi)$. Since $\psi_n/2 - \phi_{2n+1} = \Phi_0/2 - \phi_{av}$ where $\phi_{av} = (\phi_{2n+1} + \phi_{2n+2})/2$ is the average CEP, the PT amplitude (8) for this train I
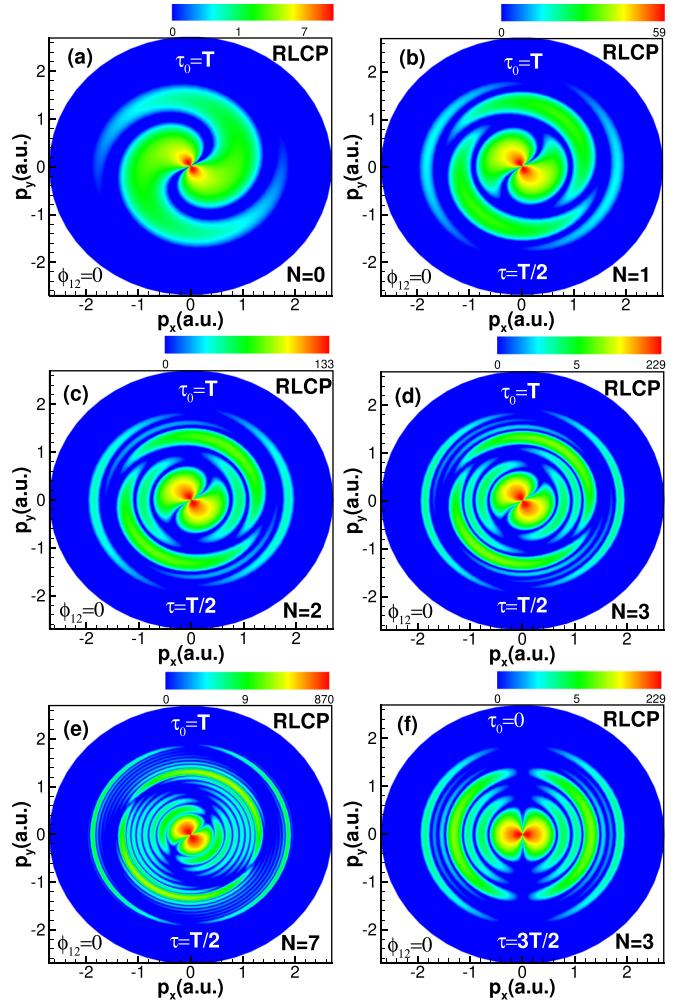


FIG. 2. TDSE results (in units of $10^{-4}$ a.u.) for the momentum distribution in the polarization plane [calculated using (2)] for photoionization of He by a train I of $N + 1$ pairs of coherent pulses with time delays $\tau_0 = T \simeq 115$ as and $\tau = T/2$ in (b)–(e) or $\tau_0 = 0$ and $\tau = 3T/2$ in (f). Parameters of the RLCP pulses in a pair are $\omega = 36$ eV, $n_c = 1$ cycle, $T = n_c(2\pi/\omega)$, $f(t) = \cos^2(\pi t/T)$, $I_0 = 10^{14}$ W/cm², and zero CEPs, i.e., $\Delta\phi_n \equiv \phi_{12} = \phi_1 - \phi_2 = 0$ for any $n$. The TDP magnitudes are indicated by the color scales.

becomes

$$
\mathcal{A} = \sqrt{2}\alpha(p)e^{i(\Phi_0/2)}\sin\theta \sum_n [e^{-i\phi_{av}}\cos(\psi_n/2 - \hat{\xi}\varphi)]q^n. \quad (9)
$$

The result (9) describes the interaction between the created $N + 1$ spiral electron vortices with the same handedness.

For one pair in train I [$N = 0$ in (9)], the TDP $\mathcal{W}(\mathbf{p}) \equiv |\mathcal{A}|^2$ reduces to the prediction [11]:

$$
\mathcal{W}(\mathbf{p}) = 2|\alpha(p)|^2 \sin^2\theta \cos^2(\psi_0/2 - \hat{\xi}\varphi), \quad (10)
$$

which leads to spiral patterns in the photoelectron momentum distribution in the polarization plane ($\theta = \pi/2$) for $\tau_0 \neq 0$, as shown in Fig. 2(a) from TDSE calculations for He atom. Here, delayed in time by $\tau_0 = T$, each pulse in a pair has $n_c = 1$ cycle with a total duration of $T \simeq 115$ as. Indeed, maxima and zeros of the kinematic factor $\cos^2(\psi_0/2 - \hat{\xi}\varphi)$

in the TDP (10) given by

$$\varphi^{\max}(E) = -\hat{\xi}[\tilde{n}\pi - \Delta\phi_0/2 - (E + E_b)\tau_0/2], \quad (11)$$

$$\varphi^0(E) = -\hat{\xi}[\tilde{n}\pi + \pi/2 - \Delta\phi_0/2 - (E + E_b)\tau_0/2], \quad (12)$$

define the Archimedean spiral equations, where $\tilde{n}$ is an integer. The handedness of spirals is dictated by the pulse helicities: it is counterclockwise for $\hat{\xi} = +1$ [Fig. 2(a)] and clockwise for $\hat{\xi} = -1$ (not shown). Such spirals have two arms as $\tilde{n} = 0, 1$ are the only possible values. As shown in [11], while $\tau_0 = 0$ leads to dipolar patterns, larger time delay $\tau_0$ results in spirals that are wound more densely.

For $N > 0$, when all the odd (even) pulses in train I are coherent, $\phi_{2n+1} \equiv \phi_1$ and $\phi_{2n+2} \equiv \phi_2$, then $\Delta\phi_n \equiv \phi_{12}$ and $\phi_{av}$ for any $n$ become constant; see, e.g., Fig 2. Thus, the term between the square bracket in (9) can be pulled out of the sum. The remaining geometric sum in (9) evaluates to $(1 - q^{N+1})/(1 - q)$ and the TDP writes

$$\mathcal{W}_N(\mathbf{p}) = \beta_N(E, \tilde{\tau})\mathcal{W}(\mathbf{p}), \quad (13)$$

where the periodic sinc function describing the interference of the $N + 1$ identical spiral electron vortices writes

$$\beta_N(E, \tilde{\tau}) = \frac{\sin^2[(N+1)(E + E_b)\tilde{\tau}/2]}{\sin^2[(E + E_b)\tilde{\tau}/2]}. \quad (14)$$

TDSE results for the momentum distributions in the polarization plane for $N = 1, 2, 3, 7$ are shown in Figs. 2(b)–2(e). For fixed time delays $\tau_0 = T$ and $\tau = T/2$, all these momentum distributions exhibit three pairs of principal (more intense) two-arm spiral patterns well separated in energy with the same handedness as in Fig. 2(b). As $N$ increases, a number of pairs of secondary (less intense) two-arm spirals appears, while the widths of principal spirals become narrower. Comparing Eqs. (10) and (13), the full understanding of these patterns requires a complete analysis of the interference factor $\beta_N(E, \tilde{\tau})$ (14).

For the cosine-square pulse envelope used here, $|\alpha(p)|^2$ in the TDP (10) for a time two-slit experiment involves the sinc-like function $J(E) \equiv |\hat{F}^+(\epsilon)|^2 = \sin^2(\epsilon T/2)/[\epsilon^2(1 - T^2\epsilon^2/4\pi^2)^2]$ so that the time-energy Fraunhofer function $J(E)\beta_N(E, \tilde{\tau})$ involved in the TDP (13) is the counterpart of the space-momentum Fraunhofer function in electron diffraction at multiple slits [7]. Note that $J(E)$ fixes the energy range for our photoionization process to be $\omega - E_b \pm \Delta\omega$. In Fig. 2 the pulse bandwidth is $\Delta\omega \simeq 1.44\omega/n_c \simeq 51.8$ eV, meaning that $0 \leqslant E \leqslant 63.2$ eV. At $\tau = T/2$ and thus $\tilde{\tau} = 3T/2 = 172.5$ as the variation with electron energy $E$ in this energy range of the interference function $\beta_N(E, \tilde{\tau})$ and the Fraunhofer function $J(E)\beta_N(E, \tilde{\tau})$, scaled by $(N + 1)^2$ for $N = 0, 1, 2, 3, 7$, is displayed in Fig. 3(a) and Fig. 3(b), respectively. For $N = 0$, $\beta_0(E, \tilde{\tau}) = 1$, see Eq. (14) and Fig. 3(a). Thus the TDPs (13) and (10) coincide, and the dash green curve in Fig. 3(b) provides a direct measurement for $J(E)$.

For $N = 1$, the function $\beta_1(E, \tilde{\tau}) = 4\cos^2[(E + E_b)\tilde{\tau}/2]$ in Fig. 3(a) exhibits in this energy range three identical broad large maxima (called principal maxima) located at $2k\pi/\tilde{\tau} - E_b$, where $k$ is an integer. From the TDP (13), one sees that these principal maxima divide the two-arm counterclockwise spiral pattern [Fig. 2(a)] to yield three pairs of principal counterclockwise two-arm spirals, shown in Fig. 2(b). For $N \geqslant 2$,
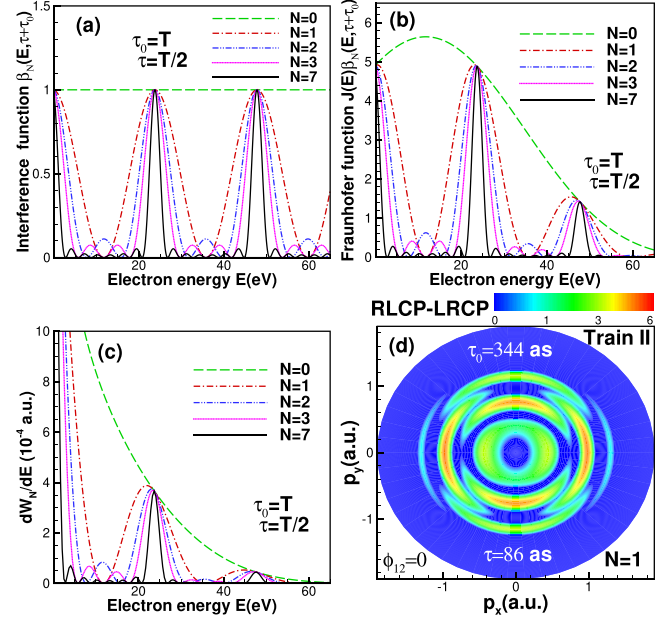


FIG. 3. Variation with energy $E$ of (a) interference factor $\beta_N(E, \tilde{\tau})$ [Eq. (14)], (b) time-energy Fraunhofer function $J(E)\beta_N(E, \tilde{\tau})$ where $J(E) \equiv |\hat{F}^+(\epsilon)|^2$, and (c) TDSE result for the SDP analyzed using (15). All these results for a one-cycle train I are scaled by $(N + 1)^2$ for $N = 0, 1, 2, 3, 7$ at a fixed $\tilde{\tau} = \tau_0 + \tau = 3T/2$. (d) shows the $(\mathbf{p}_x, \mathbf{p}_y)$ distribution by a three-cycle pulse train II for $N = 1$, $\tau_0 = 344$ as and $\tau = T/4$. In (a)–(d), $\tau_0 = T$ and the other train parameters are as in Fig. 2.

the principal maxima in $\beta_N(E, \tilde{\tau})$ shown in Fig. 3(a) are in the same positions as for the case $N = 1$; however, they are much narrower and also sharper, as reflected by the narrower widths and larger unequal intensities of the three pairs of principal spiral patterns seen in Fig. 2(c) for $N = 2$, Fig. 2(d) for $N = 3$, and Fig. 2(e) for $N = 7$. Indeed, the height of each principal maximum increases as $(N + 1)^2$; so from energy conservation the width of each principal maximum must be proportional to $1/(N + 1)$.

Between adjacent principal maxima, there are small secondary (subsidiary) maxima whose intensity becomes smaller in comparison to the principal maxima as $N$ increases. A closer look of Figs. 3(a) and 3(b) shows there are $N$ minima and $N - 1$ subsidiary maxima between adjacent principal maxima. Thus, these subsidiary structures from $\beta_N(E, \tilde{\tau})$ for $N \geqslant 2$, characteristic of diffraction grating, slice the wings of the three pairs of principal spirals to generate $N - 1$ pairs of secondary (less intense) two-arm spiral-like patterns, clearly visible in Figs. 2(c), 2(d), and 2(e). For $\tau_0 = 0$ corresponding to a linearly polarized train of attopulses similar to the one in [33], as expected from PT formula (13) the momentum distribution for $\tau = \tilde{\tau} = 3T/2$ shown in Fig. 2(f) exhibits pairs of principal and secondary waxing-waning crescent moon-like patterns. All these subsidiary features evidenced in Fig. 2 for zero or nonzero $\tau_0$ can be used for determining the number $N + 1$ of pairs of pulses in train I.

TDSE results in Fig. 2(b)–2(e) show that the intensity of the principal and secondary spiral pairs decreases as one moves radially outward in energy from the center. Let us

explain this and also control the intensity and number of these spiral pairs by analyzing the singly-differential probability (SDP) obtained by integrating the TDP (13) over the spherical angles $(\theta, \varphi)$:

$$\frac{d\mathcal{W}_N}{dE} \equiv \frac{8\pi}{3} I_0 |\mu(E)|^2 [J(E)\beta_N(E, \tilde{\tau})]. \quad (15)$$

For $N = 0$, $\beta_0(E, \tilde{\tau}) = 1$ and the dash green curve of the SDP in Fig. 3(c) thus provides a direct measurement of $|\alpha(p)|^2 = I_0 |\mu(E)|^2 J(E)$. With the single-slit modulating pattern $J(E)$ given by Fig. 3(b) for $N = 0$, one obtains that the radial matrix element $|\mu(E)|^2$ for He decreases monotonically with $E$. For $N \geqslant 1$, the energy distributions scaled by $(N + 1)^2$ present spectra characteristic to multiple slits, as exemplified in Fig. 3(c) for $N = 1, 2, 3, 7$. As $E$ increases, Fig. 3(c) shows that the intensities of the principal and secondary maxima decrease. Because $\beta_N(E, \tilde{\tau})$ (14) in Fig. 3(a) displays undamped oscillations, this decrease in intensity is a result of the single-slit modulating pattern $J(E) \propto 1/\epsilon^2$, combined with the effect of $|\mu(E)|^2$. The resulting electron grating spectra in Fig. 3(c) forms a train of electron pulses, where the composite pulses have the same width but different intensities. These features of electron pulses can be controlled. The narrower the time single slit (i.e., the shorter pulse length $T$), the broader the single-slit pattern $J(E)$ and the slower the decrease in intensity from one interference maximum to the next. The greater the value of $N$, the narrower and taller the principal maxima (electron pulses) become.

Being independent of $N$, successive principal maxima in Fig. 3(c) are separated by $2\pi/\tilde{\tau}$, providing thus a direct measure for the time delay $\tilde{\tau} \equiv \tau + \tau_0$ between successive pulse pairs. Also, the longer the value of $\tilde{\tau}$, the denser the number of oscillations and the larger the number of spiral pairs, as illustrated in Appendix A where Fig. 4 for $\tau = T/4, T, 2T$ at fixed $\tau_0 = T$ with $n_c = 3$ cycles are shown as a study for the pulse duration effect. Our analysis indicates that an isolated electron pulse with well-defined energy can be generated by using a train of pairs of pulses with large $N$, separated in time by short delay $\tilde{\tau}$, with each pulse having long duration $T$. Finally, knowing $\tilde{\tau}$ from the SDP analysis, the time delay $\tau = \tilde{\tau} - \tau_0$ can then be inferred if $\tau_0$ can be measured as in [11] by studying the time-delay sensitivity (periodicity) of the angular distributions at a fixed energy $E$. This phenomenon known as a quantum beat between the ground state and a continuum state [11] could find applications in attosecond optical switches.

All these TDSE results are for zero CEPs. Appendix B discusses the sensitivity of principal spiral pairs to the pulse CEP. For $N = 1$, Fig. 5 illustrates how the shape of spiral pairs can be controlled by varying the CEPs. For varying $\phi_3$ and other CEPs set to zero, mixing two spiral patterns that differ by a large rotation angle $\phi_3/2$ leads to a two-arm roller coaster spiral, since crests and troughs (nonzero minima) are formed along the two spiral arms.

### B. Interaction of several two-arm spiral patterns with opposite handedness

Finally, let us consider a train II of $N + 1$ pairs of coherent pulses in which two successive pairs are made of
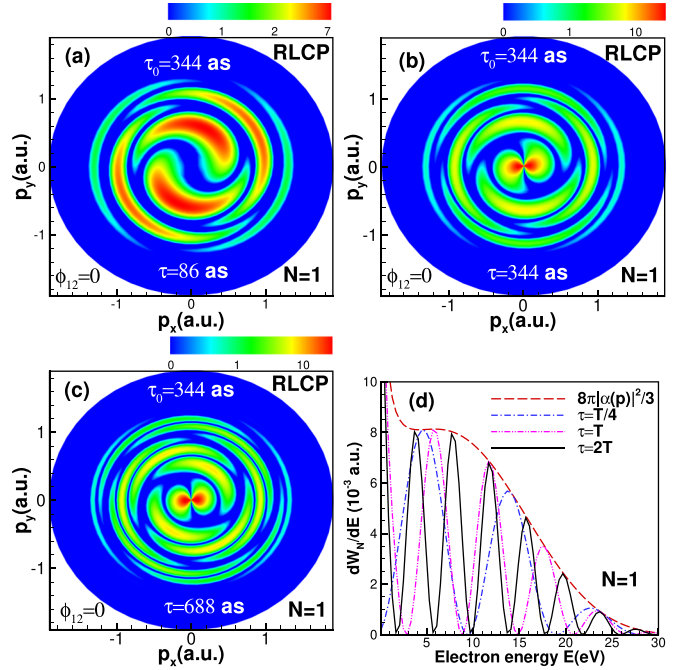


FIG. 4. Momentum distributions [calculated using Eq. (2)] in the polarization plane by a train I of two pulse pairs delayed in time by (a) $\tau = T/4$, (b) $\tau = T$, and (c) $\tau = 2T$. Panel (d) shows the singly differential probabilities [Eq. (10)] for these three values of $\tau$. In a pair, the two RLCP pulses are delayed in time by $\tau_0 = T$. Pulse parameters are $\omega = 36$ eV, $I_0 = 10^{14}$ W/cm$^2$, $n_c = 3$ cycles, $T \simeq 344$ as zero CEP and cos$^2$ envelope.

RLCP/LRCP pulses. The corresponding TDP writes

$$\mathcal{W}_N = 2I_0 |\mu(E)|^2 [J(E)\gamma_N(E, \tilde{\tau})] \sin^2 \theta$$
$$\times |\cos(\psi_0/2 - \hat{\xi}\varphi) + q\cos(\psi_0/2 + \hat{\xi}\varphi)|^2, \quad (16)$$

where $\hat{\xi} = +1(-1)$ for RLCP/LRCP (LRCP/RLCP) pulses is meaningless, and the periodic sinc function,

$$\gamma_N(E, \tilde{\tau}) = \frac{\sin^2[(N + 1)(E + E_b)\tilde{\tau}/2]}{\sin^2[(E + E_b)\tilde{\tau}]}, \quad (17)$$

can be obtained from $\beta_N(E, \tilde{\tau})$ (14) by changing $\tilde{\tau}/2$ to $\tilde{\tau}$ in the denominator. Valid for only odd values of $N$, $\gamma_N(E, \tilde{\tau})$ describes the interference of $(N + 1)/2$ identical pairs of two-arm spiral electron vortices with opposite handedness. For $N = 1$ with $n_c = 3$ cycles, $\tau_0 = T$, and $\tau = T/4$ for illustration, $\gamma_1 = 1$ and the achiral momentum distribution in the polarization plane shown in Fig. 3(d) does not lead to spiral-like patterns, but instead to crocodile-eye-like patterns including nictares composed of pairs of waxing-waning crescent moon-like patterns. For $N \geqslant 3$ and odd, this reference pattern in Fig. 3(d) is just modulated by the function $\gamma_N(E, \tilde{\tau})$. Thus, for the same energy range and fixed $\tilde{\tau}$, the number of identical broad principal maxima in Figs. 3(a)–3(c) would double. Also, while there are $(N - 1)/2$ minima and $(N - 3)/2$ subsidiary maxima, the height of each maxima increases as $(N + 1)^2/4$ and its width decreases with $N$ as $2/(N + 1)$.
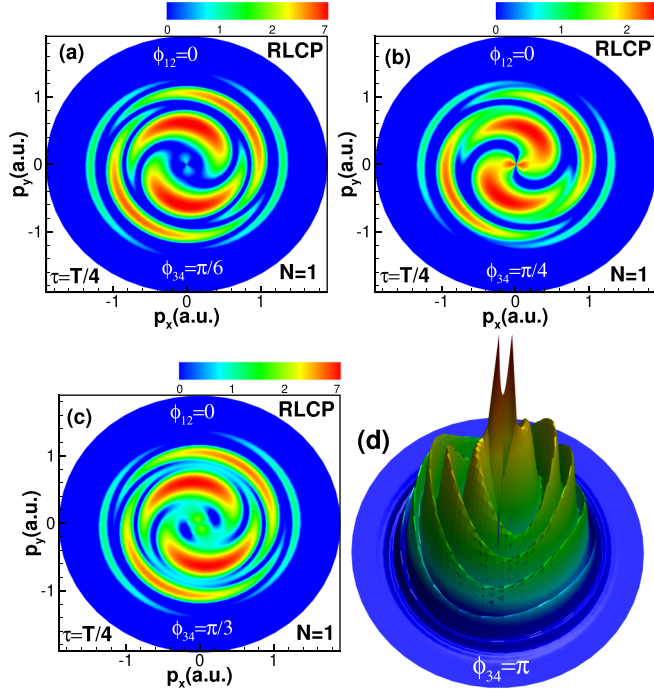
FIG. 5. Relative CEP $\phi_{34}$-sensitivity of the momentum distributions in the polarization plane by a train I of two pulse pairs delayed in time by $\tau = T/4$ for (a) $\phi_{34} = \pi/6$, (b) $\phi_{34} = \pi/4$, (c) $\phi_{34} = \pi/3$, and (d) $\phi_{34} = \pi$. In all panels, $\phi_{12} = 0$ and the other pulse parameters are the same as in Fig. 4(a).

## IV. SUMMARY AND CONCLUSIONS

In summary, using trains of pairs of counter-rotating CP pulses to photoionize any $S$-atom, interactions between several temporal two-slit interference experiments are investigated. For interaction between a pair of double-slit experiments, the helicity effect in a pulse pair is found to yield two different reference patterns, namely, pairs of principal spirals and a crocodile-eye-like pattern. When more than two double-slit experiments are involved, these two reference patterns are modulated by different kinds of time-energy Fraunhofer functions exhibiting principal and secondary maxima. Our joint TDSE and PT quantum treatments can be applied for other pulse trains such as corotating CP pulses, and complex pulse trains with ellipticity varying from pulse to pulse. Our predictions for any $S$-atom can be measured either in the femtosecond [14–17] or attosecond regime given that isolated attosecond pulses with full control of their polarization [38] exist. Also, time-delayed and tunable isolated attosecond pulses with gigawatt power seeded by a free-electron laser have been reported [39].

## APPENDIX A: SENSITIVITIES OF SPIRAL PAIRS TO THE TIME DELAY $\tau$ AND PULSE DURATION $T$

TDSE results for the momentum distributions produced by train I for $N = 1$ are discussed above for the case $n_c = 1$ cycle and time delays $\tau_0 = T \simeq 115$ as and $\tau = T/2$. In Figs. 4(a)–4(c) we show TDSE results for $N = 1$ but for longer pulse duration $T \simeq 344$ as (corresponding to $n_c = 3$ cycles) and time delay $\tau_0 = T$. While the momentum distribution in Fig. 4(a) is for shorter pulse pair time delay $\tau = T/4$, those in Figs. 4(b) and 4(c) are for longer pulse pair time delays, $\tau = T$ and $\tau = 2T$, respectively. To ease analyses of these patterns, plotted in Fig. 4(d) are the singly differential probabilities (SDPs) for these three values of $\tau$. One sees that the longer the value of $\tilde{\tau} = \tau_0 + \tau$, the denser the number of oscillations in the SDP; see Fig. 4(d) where $\tilde{\tau} = 5T/4, 2T, 3T$. Note that larger number of oscillations implies larger number of principal maxima, which yields larger number of pairs of principal spirals. Figures 4(a)–4(c) show that this is indeed the case, since the momentum distribution in Fig. 4(a) exhibits three pairs of principal spirals, while those in Fig. 4(b) and Fig. 4(c) present, respectively, five and seven pairs of principal spirals, reflecting thus the number of principal maxima in Fig. 4(d) for these three values of time delay $\tau$.

Let us compare Fig. 2(b) with Fig. 4(a), where the former is produced by one-cycle pulses and the latter by three-cycle pulses. One sees that increasing the pulse length from one to three cycles reduces the pulse bandwidth from 51.84 eV to 17.28 eV. Consequently, the energy range within which the electron energy varies shrinks from $0 \leqslant E \leqslant 63.24$ eV to $0 \leqslant E \leqslant 28.68$ eV. However, for $\tilde{\tau} = 3T/2$ and $\tilde{\tau} = 5T/4$ used in these two cases, the SDPs in Fig. 3(c) together with Fig. 4(d) for $\tau = T/4$ exhibits three principal maxima in each case within these two different energy ranges. Therefore, this results in three pairs of principal spirals as shown in both Fig. 2(b) and Fig. 4(a). The difference observed between the two patterns is due to the difference in the locations, $2k\pi/\tilde{\tau} - E_b$, of these principal maxima.

## APPENDIX B: SENSITIVITY OF SPIRAL PAIRS TO THE PULSE CEP

All TDSE results shown above are for zero CEPs so that $\phi_{12} \equiv \phi_1 - \phi_2 = 0$ and $\phi_{34} \equiv \phi_3 - \phi_4 = 0$. Here we study how the spiral pairs in Fig. 4(a) produced by train I for $N = 1$ is sensitive to the CEPs of the pulses in train I. The ionization amplitude (describing the interaction of a pair of two-arm spiral patterns with the same handedness) produced by two pulse pairs with arbitrary CEPs, $\phi_1, \phi_2, \phi_3$, and $\phi_4$, is

$$\mathcal{A} \simeq \sqrt{2}\alpha(p)\sin\theta\, e^{i\Phi_0/2}\{q_{12}\cos[(\Phi_0 + \phi_{12})/2 - \xi\varphi]$$
$$+ q_{34}\cos[(\Phi_0 + \phi_{34})/2 - \xi\varphi]\}, \tag{B1}$$

where $q_{12} = e^{-i(\phi_1 + \phi_2)/2}$ and $q_{34} = e^{i[\tilde{\Phi}_1 - (\phi_3 + \phi_4)/2]}$. Shown in Fig. 5 are results for $\phi_1 = \phi_2 = \phi_4 = 0$ with $\phi_3$ varying and taking the values 0 in Fig. 4(a), $\pi/6$ in Fig. 5(a), $\pi/4$ in Fig. 5(b), $\pi/3$ in Fig. 5(c), and $\pi/2$ in Fig. 5(d). Since $\phi_{12} = 0$ and $\phi_{34}$ varies, the two-arm spiral pattern described by $\cos[(\Phi_0 + \phi_{34})/2 - \xi\varphi]$ in (B1) can be obtained from the two-arm spiral pattern described by $\cos[(\Phi_0 + \phi_{12})/2 - \xi\varphi]$

by means of a counterclockwise rotation of $\phi_{34}/2$. When these two spiral patterns are mixed due to the interference phase factor $q_{34}$ involving $\phi_3$ and the Ramsey phase $\tilde{\Phi}_1$, the ends and beginnings of neighboring spiral pairs merge, as evidenced by Figs. 5(a) and 5(b) for small angles $\phi_{34} = \pi/6, \pi/4$. In the

interference course for larger angles $\phi_{34} \geqslant \pi/3$, crests and troughs (nonzero minima) are thus formed along the two arms of the spiral leading to a two-arm roller coaster spiral when visualized in three dimensions [Fig. 5(d) for $\phi_{34} = \pi$] or in two dimensions [Fig. 5(c) for $\phi_{34} = \pi/3$].

[1] T. Young, *A Course of Lectures on Natural Philosophy and Mechanical Arts* (Johnson, London, 1807).

[2] A. Einstein, Über einen die Erzeugung und Verwandlung des Lichtes betreffenden heuristischen Gesichtspunkt, Ann. Phys. **17**, 132 (1905).

[3] A. H. Compton, A quantum theory of the scattering of X-rays by light elements, Phys. Rev. **21**, 483 (1923).

[4] L. de Broglie, The reinterpretation of wave mechanics, Found. Phys. **1**, 5 (1970).

[5] C. Davisson and L. H. Germer, Diffraction of electrons by a crystal of nickel, Phys. Rev. **30**, 705 (1927).

[6] C. Jönsson, Elektroneninterferenzen an mehreren künstlich hergestellten Feinspalten, Z. Phys. **161**, 454 (1961).

[7] C. Jönsson, Electron diffraction at multiple slits, Am. J. Phys. **42**, 4 (1974).

[8] M. Wollenhaupt *et al.*, Interferences of Ultrashort Free Electron Wave Packets, Phys. Rev. Lett. **89**, 173001 (2002).

[9] F. Lindner *et al.*, Attosecond Double Slit Experiment, Phys. Rev. Lett. **95**, 040401 (2005).

[10] N. F. Ramsey, A molecular beam resonance method with separated oscillating fields, Phys. Rev. **78**, 695 (1950).

[11] J. M. Ngoko Djiokap, S. X. Hu, L. B. Madsen, N. L. Manakov, A. V. Meremianin, and A. F. Starace, Electron Vortices in Photoionization by Circularly Polarized Attosecond Pulses, Phys. Rev. Lett. **115**, 113004 (2015).

[12] J. M. Ngoko Djiokap, A. V. Meremianin, N. L. Manakov, S. X. Hu, L. B. Madsen, and A. F. Starace, Multistart spiral electron vortices in ionization by circularly polarized UV pulses, Phys. Rev. A **94**, 013408 (2016).

[13] M. Harris, C. A. Hill, and J. M. Vaughan, Optical helices and spiral interference fringes, Opt. Commun. **106**, 161 (1994).

[14] D. Pengel, S. Kerbstadt, D. Johannmeyer, L. Englert, T. Bayer, and M. Wollenhaupt, Electron Vortices in Femtosecond Multiphoton Ionization, Phys. Rev. Lett. **118**, 053003 (2017).

[15] D. Pengel, S. Kerbstadt, L. Englert, T. Bayer, and M. Wollenhaupt, Control of three-dimensional electron vortices from femtosecond multiphoton ionization, Phys. Rev. A **96**, 043426 (2017).

[16] S. Kerbstadt, K. Eickhoff, T. Bayer, and M. Wollenhaupt, Odd electron wave packets from cycloidal ultrashort laser fields, Nat. Commun. **10**, 658 (2019).

[17] S. Kerbstadt, K. Eickhoff, T. Bayer, and M. Wollenhaupt, Control of free electron wave packets by polarization-tailored ultrashort bichromatic laser fields, Adv. Phys.: X **4**, 1672583 (2019).

[18] K.-J. Yuan, S. Chelkowski, and A. D. Bandrauk, Photoelectron momentum distributions of molecules in bichromatic circularly polarized attosecond UV laser fields, Phys. Rev. A **93**, 053425 (2016).

[19] K.-J. Yuan, H. Lu, and A. D. Bandrauk, Photoionization of triatomic molecular ions $H_3^{2+}$ by intense bichromatic circularly polarized attosecond UV laser pulses, J. Phys. B **50**, 124004 (2017).

[20] J. M. Ngoko Djiokap, A. V. Meremianin, N. L. Manakov, S. X. Hu, L. B. Madsen, and A. F. Starace, Kinematical vortices in double photoionization of helium by attosecond pulses, Phys. Rev. A **96**, 013405 (2017).

[21] J. M. Ngoko Djiokap and A. F. Starace, Doubly-excited state effects on two-photon double ionization of helium by time-delayed, oppositely circularly-polarized attosecond pulses, J. Opt. **19**, 124003 (2017).

[22] Z. L. Li, Y. J. Li, and B. S. Xie, Momentum vortices on pairs production by two counter-rotating fields, Phys. Rev. D **96**, 076010 (2017).

[23] M. Li, G. Zhang, T. Zhao, X. Ding, and J. Yao, Electron vortices in photoionization by a pair of elliptically polarized attosecond pulses, Chin. Opt. Lett. **15**, 120202 (2017).

[24] M. Li, G. Zhang, X. Kong, T. Wang, X. Ding, and J. Yao, Dynamic Stark induced vortex momentum of hydrogen in circular fields, Opt. Express **26**, 878 (2018).

[25] X. Kong, G. Zhang, M. Li, T. Wang, X. Ding, and J. Yao, Odd-fold-symmetric spiral momentum distributions and their Stark distortions in hydrogen, J. Opt. Soc. Am. B **35**, 2163 (2018).

[26] J. M. Ngoko Djiokap, A. V. Meremianin, N. L. Manakov, L. B. Madsen, S. X. Hu, and A. F. Starace, Dynamical electron vortices in attosecond double photoionization of $H_2$, Phys. Rev. A **98**, 063407 (2018).

[27] X.-R. Xiao, M.-X. Wang, H. Liang, Q. Gong, and L.-Y. Peng, Proposal for Measuring Electron Displacement Induced by a Short Laser Pulse, Phys. Rev. Lett. **122**, 053201 (2019).

[28] L. Geng, F. C. Vélez, J. Z. Kamiński, L.-Y. Peng, and K. Krajewska, Vortex structures in photodetachment by few-cycle circularly polarized pulses, Phys. Rev. A **102**, 043117 (2020).

[29] J. M. Ngoko Djiokap, A. V. Meremianin, and N. L. Manakov, Electron interference in atomic ionization by two crossing polarized ultrashort pulses, Phys. Rev. A **103**, 023103 (2021).

[30] J. M. Ngoko Djiokap and A. F. Starace, Temporal coherent control of resonant two-photon double ionization of the hydrogen molecule via doubly excited states, Phys. Rev. A **103**, 053110 (2021).

[31] T. Zuo and A. D. Bandrauk, High-order harmonic generation in intense laser and magnetic fields, J. Nonlin Opt. Phys. Mater. **4**, 533 (1995).

[32] D. Baykusheva, S. Brennecke, M. Lein, and H. J. Wörner, Signatures of Electronic Structure in Bicircular High-Harmonic Spectroscopy, Phys. Rev. Lett. **119**, 203201 (2017).

[33] P. M. Paul, E. S. Toma, P. Breger, G. Mullot, F. Auge, Ph. Balcou, H. G. Muller, and P. Agostini, Observation of a train

of attosecond pulses from high harmonic generation, Science **292**, 1689 (2001).

[34] E. A. Pronin, A. F. Starace, M. V. Frolov, and N. L. Manakov, Perturbation theory analysis of attosecond photoionization, Phys. Rev. A **80**, 063403 (2009).

[35] J. M. Ngoko Djiokap, N. L. Manakov, A. V. Meremianin, S. X. Hu, L. B. Madsen, and A. F. Starace, Nonlinear Dichroism in Back-to-Back Double Ionization of He by an Intense Elliptically Polarized Few-Cycle Extreme Ultraviolet Pulse, Phys. Rev. Lett. **113**, 223002 (2014).

[36] J. M. Ngoko Djiokap, S. X. Hu, W.-C. Jiang, L.-Y. Peng, and A. F. Starace, Enhanced asymmetry in few-cycle attosecond pulse ionization of He in the vicinity of autoionizing resonances, New J. Phys. **14**, 095010 (2012).

[37] A. S. Davydov, *Quantum Mechanics*, 2nd ed. (Pergamon Press, Oxford, 1976).

[38] P.-C. Huang *et al.*, Polarization control of isolated high-harmonic pulses, Nat. Photonics **12**, 349 (2018).

[39] J. Duris *et al.*, Tunable isolated attosecond X-ray pulses with gigawatt peak power from a free-electron laser, Nat. Photon. **14**, 30 (2020).